Pushing the boundaries of chemistry? It takes #HumanChemistry

Make your curiosity and talent as a chemist matter to the world with a specialty chemicals leader. Together, we combine cutting-edge science with engineering expertise to create solutions that answer real-world problems. Find out how our approach to technology creates more opportunities for growth, and see what chemistry can do for you at:

evonik.com/career

EVONIK
Leading Beyond Chemistry

ADVANCED FUNCTIONAL MATERIALS
www.afm-journal.de

Glassy Metal–Organic-Framework-Based Quasi-Solid-State Electrolyte for High-Performance Lithium-Metal Batteries

Guangshen Jiang, Changzhen Qu, Fei Xu, En Zhang, Qiongqiong Lu, Xiaoru Cai, Steffen Hausdorf, Hongqiang Wang,* and Stefan Kaskel**

Enhancing ionic conductivity of quasi-solid-state electrolytes (QSSEs) is one of the top priorities, while conventional metal–organic frameworks (MOFs) severely impede ion migration due to their abundant grain boundaries. Herein, ZIF-4 glass, a subset of MOFs, is reported as QSSEs (LGZ) for lithium-metal batteries. With lean Li content (0.12 wt%) and solvent amount (19.4 wt%), LGZ can achieve a remarkable ion conductivity of 1.61×10^{-4} S cm^{-1} at 30 °C, higher than those of crystalline ZIF-4-based QSSEs (LCZ, 8.21×10^{-5} S cm^{-1}) and the reported QSSEs containing high Li contents (0.32–5.4 wt%) and huge plasticizer (30–70 wt%). Even at −56.6 °C, LGZ can still deliver a conductivity of 5.96×10^{-6} S cm^{-1} (vs 4.51×10^{-7} S cm^{-1} for LCZ). Owing to the grain boundary-free and isotropic properties of glassy ZIF-4, the facilitated ion conduction enables a homogeneous ion flux, suppressing Li dendrites. When paired with $LiFePO_4$ cathode, LGZ cell demonstrates a prominent cycling capacity of 101 mAh g^{-1} for 500 cycles at 1 C with the near-utility retention, outperforming LCZ (30.7 mAh g^{-1}) and the explored MOF-/covalent–organic frameworks (COF)-based QSSEs. Hence, MOF glasses will be a potential platform for practical quasi-solid-state batteries in the future.

1. Introduction

Metal–organic frameworks (MOFs) have emerged as a type of crystalline porous materials (CPMs) with long-range order as well as the well-organized coordination bonds between target-designed metal ions and organic building blocks.[1] These distinct features empower MOFs with promising applications in gas adsorption/separation,[2] drug delivery,[3] and catalysis.[4] Apart from these, they are recently employed as prominent platforms for designing quasi-solid-state electrolytes (QSSEs) because of their electrically insulating nature as well as facile processability.[5] As an intermediate between liquid and all-solid-state electrolytes, QSSEs usually incorporate Li salt into organic solvent, helping it to dissociate ion pairs and promote Li^+ conduction as a plasticizer.[6] In principle, certain amounts of Li salt and solvent are required to afford sufficient ionic conductivity. Nevertheless, excessive increasing Li salt and solvent contents would enhance cost and reduce mechanical strength as well as sacrifice energy density of devices. A survey of references shows that the state-of-the-art crystalline porous frameworks such as MOF-based or covalent–organic frameworks (COF)-based QSSEs generally contain high Li contents (0.32–5.4 wt%) and huge proportions of the plasticizer (30–70 wt%) to ensure smooth ion conduction, such as 1.38 wt% Li and 70 wt% propylene carbonate (PC) for MIT-20,[5d] and 0.72 wt% Li and 55 wt% PC for Li^+/ICOF-2.[7] We envisage that one possible reason for such high Li and solvent contents is that the employed MOFs/COFs mainly consist of polycrystals with a multitude of grain boundaries, which would be unfavorable for ions hopping among the boundaries and impede their rapid motion. Although single-crystal CPMs including COFs and MOFs can address the problem theoretically, their implementation in batteries is not practical as their synthesis is difficult, time-consuming, and of low yield.[8] Therefore, achieving high ionic conductivity CPM-based QSSEs with low Li (<0.32 wt%) and lean solvent (<20 wt%) remains challenging, but is highly desirable.

Currently, emerged as a new class of MOF materials, MOF glasses are unique in that they have no grain boundary and thus attract scientific interests.[9] For example, glassy MOFs have been demonstrated to exhibit excellent gas separation

G. Jiang, C. Qu, F. Xu, H. Wang
State Key Laboratory of Solidification Processing
School of Materials Science and Engineering
Shaanxi Joint Laboratory of Graphene (NPU)
Northwestern Polytechnical University
Xi'an 710072, P. R. China
E-mail: feixu@nwpu.edu.cn; hongqiang.wang@nwpu.edu.cn
G. Jiang, F. Xu, E. Zhang, X. Cai, S. Hausdorf, S. Kaskel
Department of Inorganic Chemistry
Technische Universität Dresden
Bergstr. 66, 01062 Dresden, Germany
E-mail: stefan.kaskel@tu-dresden.de
Q. Lu
Leibniz IFW Dresden
Helmholtzstr. 20, 01069 Dresden, Germany

The ORCID identification number(s) for the author(s) of this article can be found under https://doi.org/10.1002/adfm.202104300.

DOI: 10.1002/adfm.202104300

properties because of eliminating grain boundary for enhancing sieving effect.[10] It could thus be envisioned that MOF glasses can afford the prospective for producing high-performance QSSEs, taking into account of their prominent ionic conductivity and isotropy without grain boundaries.[11] However, to the best of our knowledge, developing MOF glasses as QSSEs remains a critical yet unexplored field.

Herein, we introduce glassy ZIF-4 combined with lithium bis(trifluoromethanesulfonyl)imide (LiTFSI) as QSSEs and explore their potentials in lithium-metal batteries (LMBs). Li salt and solvent contents were investigated, and G-ZIF-4-based QSSEs (denoted as LGZ) exhibit a remarkable ion conductivity of 1.61×10^{-4} S cm^{-1} at 30 °C, whereas crystalline ZIF-4-based QSSEs (denoted as LCZ) shows an inferior ionic conductivity of 8.21×10^{-5} S cm^{-1} under an optimized and ultralow Li content (0.12 wt%) and solvent amount (19.4 wt%). Impressively, LGZ permits an ionic conductivity of 5.96×10^{-6} S cm^{-1} at −56.6 °C while LCZ merely allows 4.51×10^{-7} S cm^{-1}, elucidating the potential for low-temperature LMBs. LGZ shows a stable electrochemical window of 2.3–4.0 V owing to the outstanding stability of imidazole groups under electrochemistry conditions.[12] Moreover, LGZ also displays an excellent dendrite suppression and interface compatibility substantiated by plating/stripping tests for 500 h at 0.05 mA cm^{-2} and even at a higher current density of 0.1 mA cm^{-2} in contrast with LCZ. As a demonstration in Li|LGZ|LiFePO$_4$ full cell, LGZ delivers a high and stable specific capacity of 101 mAh g^{-1} at 1 C for 500 cycles with a capacity retention of near 100%, far exceeding LCZ (i.e., 30.7 mAh g^{-1}). Our proposed LGZ with low Li content and solvent amount as QSSEs is promising for lightweight and high-energy-density quasi-solid-state batteries. Meanwhile, LGZ also shows a prominent flameproof property, which is intriguing toward practical applications. The vitrified MOFs are a promising research field and may open a new avenue to obtain safe and high-performance QSSEs.

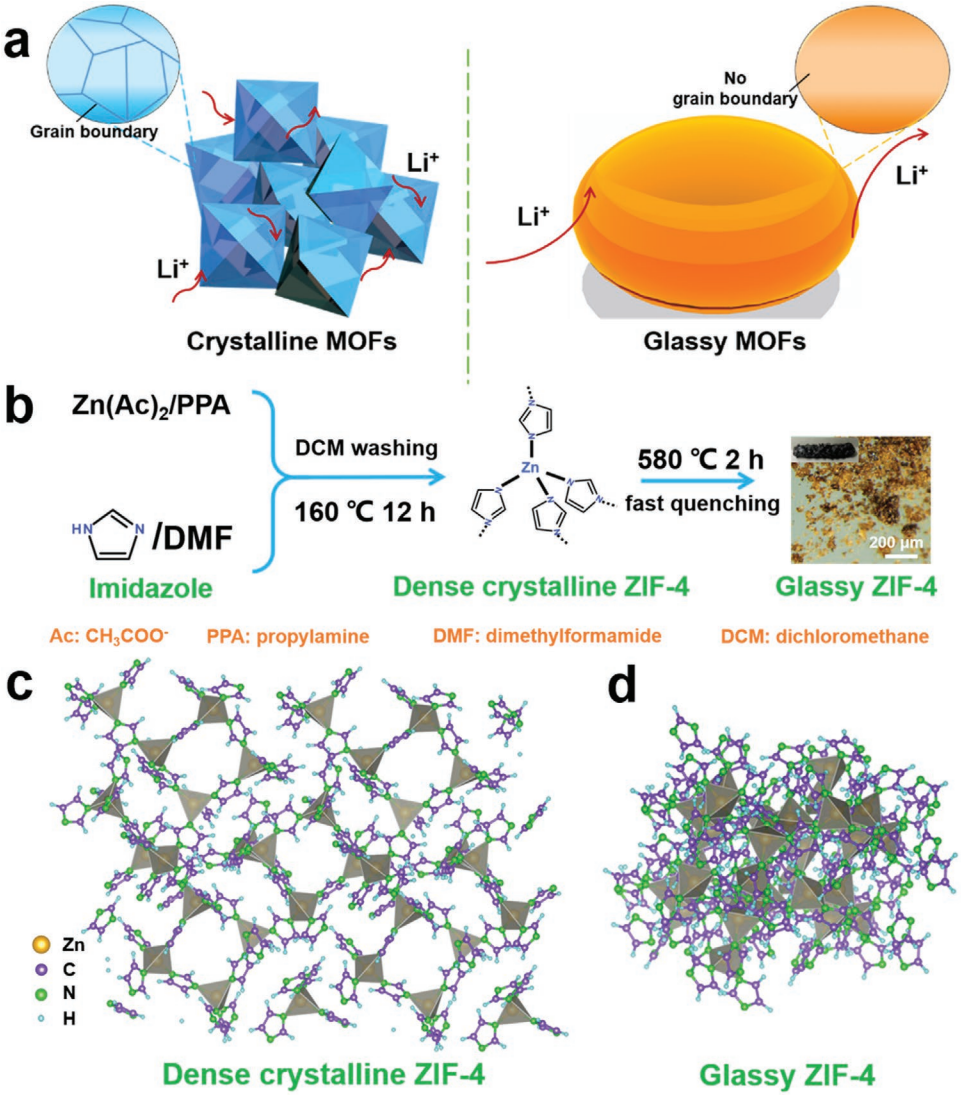

Figure 1. a) Illustration of Li ions' conduction in crystalline and glassy MOFs. b) Scheme of the preparation process for glassy ZIF-4 (inset: glassy ZIF-4 block). c,d) Molecular structure models of c) dense crystalline ZIF-4 and d) glassy ZIF-4, respectively.

2. Results and Discussion

2.1. Characterizations of Glassy ZIF-4

The ionic conduction of QSSEs is one of important factors determining the performance of quasi-solid-state batteries. As depicted in **Figure 1**a, the polycrystalline trait in most of MOFs induces sluggish ions' migration due to the blocking nature of the grain boundaries,[13] limiting MOFs' access as promising QSSEs. In contrast, materials in glassy state are featured by grain boundary-free and isotropic characteristics, and thus are expected to ensure unobstructed ions' migration. For instance, lithium-ion-conducting glass–ceramic (LICGC) Li_2O–Al_2O_3–SiO_2–P_2O_5–TiO_2 is one of potential solid electrolyte candidates with favorable Li^+ conductivity exceeding 10^{-4} S cm^{-1}.[14] In view of the overwhelming merits of glassy materials in ionic conductivity,[15] MOF glasses are deemed to own promising prospect as QSSEs for LMBs.

MOF glasses are generally formed via solid–liquid transition and the subsequent fast quenching of the corresponding liquid MOFs.[16] As illustrated in Figure 1b, ZIF-4 glass was initially prepared by the reaction of $Zn(Ac)_2$ and imidazole[17] to form porous crystalline ZIF-4, and then was transformed into dense crystalline ZIF-4 phase via desolvation,[18] followed by fast melt-quenching treatment. Typically, porous crystalline ZIF-4 is a crystalline network with connected tetrahedral geometry, as illustrated in Figure S1a (Supporting Information). X-ray diffraction (XRD) pattern shows the strong diffraction peaks of porous crystalline ZIF-4, representing a high degree of crystallinity (Figure S1b, Supporting Information), in accordance with the characteristic powder pattern of simulated ZIF-4.[19] Upon the removal of dimethyl formamide (DMF) with dichloromethane (DCM) washing, porous crystalline ZIF-4 then transforms into another crystal phase,[18] dense crystalline ZIF-4 (Figure 1c). After the final melt quenching, the original ordered crystal structure becomes disordered, implying dense crystalline ZIF-4 has evolved into glassy ZIF-4 (Figure 1d).

To further confirm the occurrence of vitrification, differential scanning calorimetry (DSC) was employed to monitor the enthalpic responses to the phase transition processes. For dense crystalline ZIF-4, amorphization and crystallization to ZIF-*zni* (the densest phase of the known ZIF-4)[18,20] occur at 307 and 488 °C, respectively, and subsequent melting at 578 °C in the initial upscan (**Figure 2**a). During the melt-quenching

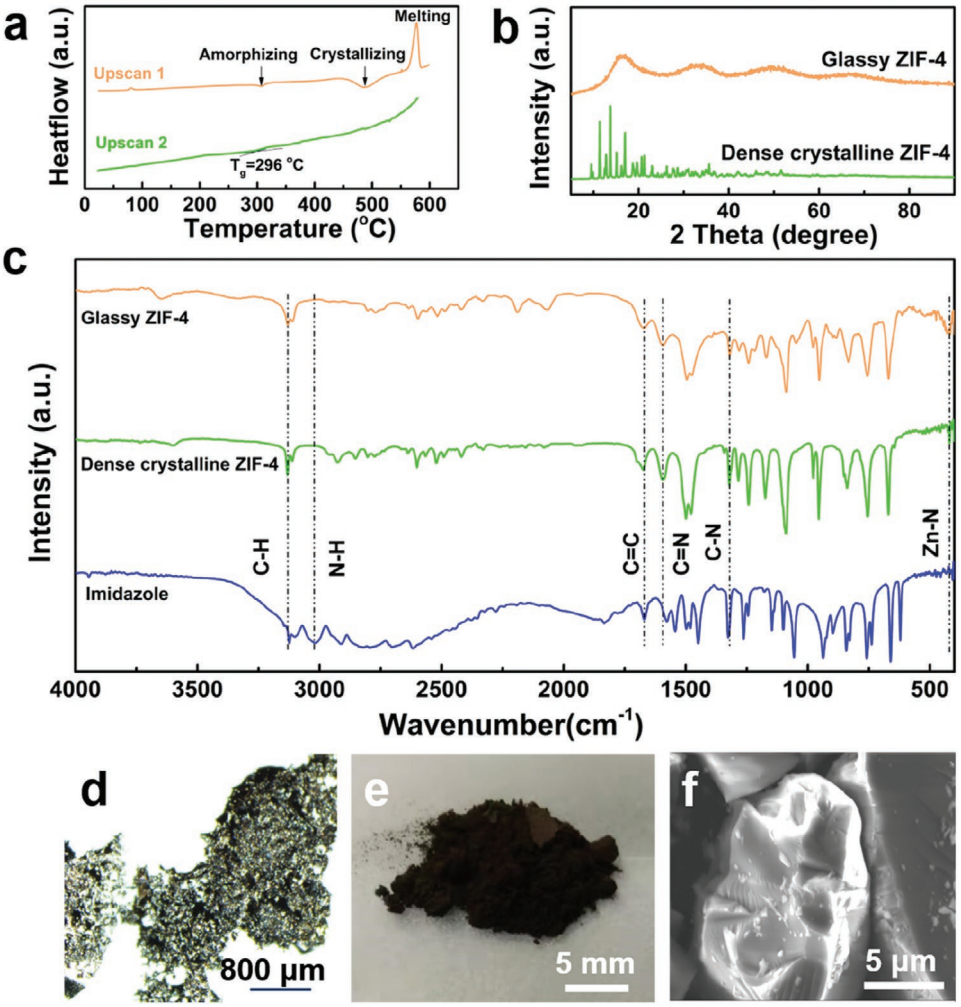

Figure 2. a) DSC upscans of dense crystalline ZIF-4. b) XRD patterns of glassy ZIF-4 and dense crystalline ZIF-4. c) IR spectra of glassy ZIF-4, dense crystalline ZIF-4, and imidazole. d) Optical microscopy image of glass ZIF-4 block. e,f) Photo and SEM image of glassy ZIF-4 after grinding.

process, ZIF-*zni* melt is vitrified and the obtained glass exhibits glass transition (T_g) at 296 °C during the second upscan. The achieved T_g is similar to the reported values.[16a,21] The XRD pattern shows that dense crystalline ZIF-4 possesses intensive characteristic peaks,[18] suggesting high crystallinity (Figure 2b). After melt-quenching treatment, the sharp peaks attributed to dense crystalline ZIF-4 disappear, and another new four broad peaks emerge (Figure 2b), further illustrating the formation of glassy phase, i.e., glassy ZIF-4. This is in agreement with the reported glassy ZIF-4.[9a] And the as-obtained ZIF-4 glass turns into a black block and appears radiant at magnified conditions (Figures 1b and 2d), in contrast to dense crystalline ZIF-4 showing as a white powder (Figure S2a,b, Supporting Information). After grinding, glassy ZIF-4 displays a deep brown color and is agglomerated into transparent and glassy particles (Figure 1b). The phase transformation from crystal into glass state involves the structural tortuosity and deformation of the entire crystal structure as well as local molecular motion, thus generating disordered structure and eliminating the crystal grain boundaries.[9a,16a] N_2 adsorption/desorption isotherms reveal an open type in dense crystalline ZIF-4 with a pore volume of 0.169 $cm^3\ g^{-1}$ and a low Brunauer–Emmett–Teller (BET) surface area of 24.8 $m^2\ g^{-1}$ (Figure S3a and Table S1, Supporting Information). Due to the structural densification and contraction at higher temperature, glassy ZIF-4 also bears open isotherms, but only a pore volume of 0.0074 $cm^3\ g^{-1}$ and a low BET surface area of 3.8 $m^2\ g^{-1}$ (Figure S3b and Table S1, Supporting Information), which is comparable to the value (2.9 $m^2\ g^{-1}$) of ZIF-4 glass reported by Bennett's group.[16a] Evidently, the BET surface area of glassy ZIF-4 is evidently lower than those of many previously reported MOFs and COFs, e.g., MIT-20 (2066 $m^2\ g^{-1}$),[5d] HKUST-1 (1150 $m^2\ g^{-1}$),[22] and ICOF-2 (1259 $m^2\ g^{-1}$).[7]

As observed from Figure 2c, dense crystalline ZIF-4 and glassy ZIF-4 have similar Fourier transform infrared (FTIR), demonstrating that only physical transformation during the melt-quenching process occurs without influencing their chemical structures. The stretching vibrations of C—H (≈3127 cm^{-1}), C=C (≈1670 cm^{-1}), C=N (≈1592 cm^{-1}), and C—N (≈1315 cm^{-1}) bands from imidazole building unit[23] remain in both crystalline and glassy ZIF-4. Moreover, the disappearance of N—H band (≈3021 cm^{-1}) and the emergence of Zn—N stretch (≈423 cm^{-1})[24] confirm the chemical coordination between imidazole and $Zn(Ac)_2$. Slight carbonization occurs (Figure S4, Supporting Information), presumably due to the decomposition of highly active uncoordinated dangling bonds at the edges of ZIF-4 surface based on the high thermal stability of ZIF-4. The scanning electron microscopy (SEM) image reveals that dense crystalline ZIF-4 is present in irregular particles (Figure S5a, Supporting Information), whereas glassy ZIF-4 resembles blocky shape (Figure 2f). Energy dispersive spectra (EDS) mappings reveal that C, N, and Zn elements are uniformly distributed in dense crystalline ZIF-4 and glassy ZIF-4, respectively (Figures S5b–d and S6, Supporting Information).

2.2. Preparation and Ionic Conductivity of LGZ

LGZ and LCZ electrolyte films were prepared by the grinding and rolling process (see the Supporting Information). The thicknesses

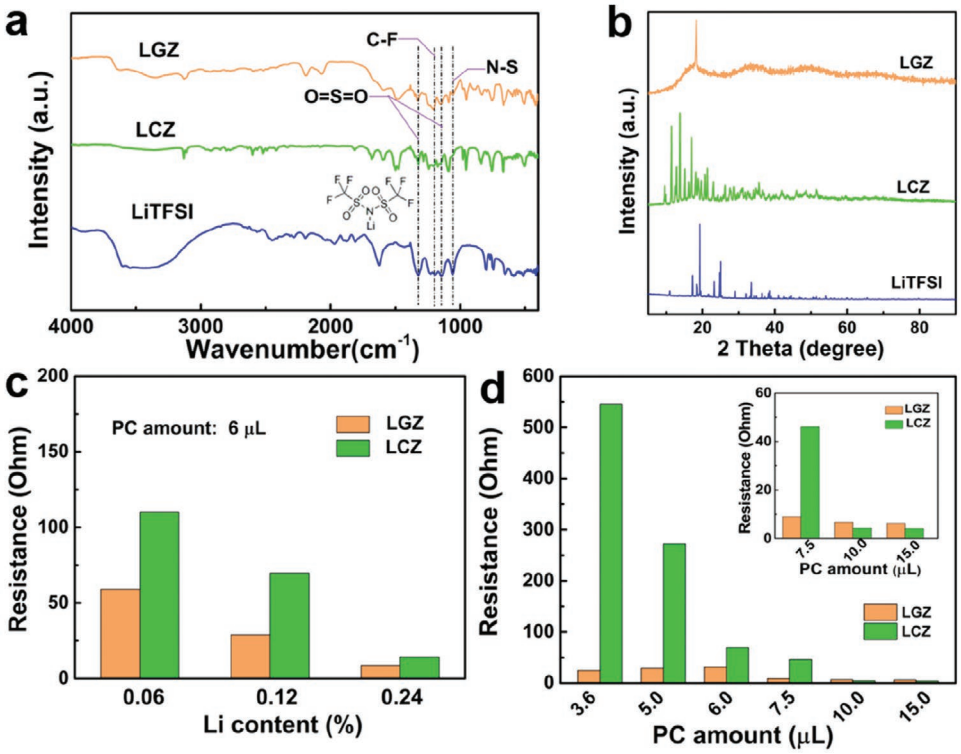

Figure 3. a) IR spectra and b) XRD patterns of LGZ, LCZ, and LiTFSI. c,d) Effects of c) Li content and d) PC amount on ionic resistance of LGZ and LCZ (inset: enlarged figure from 7.5–15 μL), respectively.

of all QSSE films were controlled to ≈100 µm (Figure S7, Supporting Information). To prove the existence of LiTFSI in QSSE films, the absorption bands of O=S=O (1334 and 1142 cm^{-1}), C−F (1196 cm^{-1}), and S−N−S (1060 cm^{-1}) assigned to $TFSI^-$ anions[25] are observed in FTIR spectra of both LGZ and LCZ (**Figure 3**a). On the other hand, the intense characteristic diffraction peaks attributed to LiTFSI emerge in both two films, further confirming the formation of QSSEs (Figure 3b). Ion conductivity was investigated by electrochemical impedance spectroscopy (EIS) in ss|QSSEs|ss (ss: stainless steel) configuration. Li^+ conductivity is closely related to Li salt and solvent contents in the QSSEs. In order to maximize the utilization of the loaded Li element, Li loading in LGZ was first optimized. By increasing the Li content, the ionic resistances of LCZ and LGZ decrease with the fixed PC volume of 6 µL at 30 °C, as is revealed in Figure 3c. Although the ionic resistance of electrolytes decreases as the concentration of carrier ions increases, the incremental dosage of expensive Li salt undeniably raises the fabrication cost of quasi-solid-state batteries. Particularly, the resistance of ion migration for LGZ is always markedly lower than that of LCZ under the same Li loading. Under a low Li content of 0.12 wt%, the resistance value of LCZ (i.e., 69.7 Ω) is almost 2.5 times higher compared with LGZ (i.e., 28.9 Ω), which would make a difference regarding to the electrochemical performance of QSSEs. On the other hand, solvents such as PC are often employed to dissolve Li salt for loading-type QSSEs,[22,26] and the effect of PC amount on ionic resistance was also studied as well with a fixed Li content of 0.12 wt%. As the PC amount increases from 3.6 to 7.5 µL, the resistance of LCZ is significantly reduced, as revealed in Figure 3d and in Figure S8 (Supporting Information). Instead, only a slight increment occurs for LGZ from 3.6 to 6 µL and a dramatical decrease at 7.5 µL. When the employed volume of PC is ≥10 µL, LCZ has lower resistances probably due to the porous structure of dense crystalline ZIF-4 (total pore volume = 0.0143 cm^3) filled with PC, which facilitates ion migration in contrast with LGZ (inset of Figure 3d). Based on the investigations above, an optimized Li loading (0.12 wt%) and a PC volume (6 µL) are selected for the subsequent studies, and LGZ and LCZ are used as the as-obtained QSSEs by utilizing glassy ZIF-4 and dense crystalline ZIF-4 matrices, respectively, unless otherwise stated.

The EIS performances under varying temperatures were also investigated. For all Nyquist plots from 30 to 80 °C, the absence of the semicircle and only linear part in the whole tested frequency range were observed. And the resistance of LGZ is lower than those of LCZ, indicating the faster ionic conduction of LGZ as QSSEs, as shown in **Figure 4**a and in Figure S9a (Supporting Information). The temperature-dependent ionic conductivity relationships ($\log\sigma = -\frac{E_a}{2.303R}\frac{1}{T} + C$, where σ: ionic conductivity (S cm^{-1}); E_a: activation energy (eV); R: molar gas constant (8.314 J mol^{-1} K^{-1}); T: thermodynamic temperature (K); and C: constant) of LGZ and LCZ are plotted in Figure 4b and in Figure S9b (Supporting Information). For LGZ, the calculated ion conductivities are calculated to be 1.61×10^{-4} and 5.26×10^{-4} S cm^{-1} at 30 and 80 °C, respectively, whereas LCZ has ion conductivities of only 8.21×10^{-5} and 1.59×10^{-4} S cm^{-1} under the same conditions correspondingly. These achieved values are also higher than those of previously reported CPMs such as MOF-/COF-based QSSEs with higher Li content and more solvent/plasticizer, e.g., Im–COF–TFSI@Li (2.92×10^{-5} S cm^{-1})[27] and polyethylene glycol/Li^+/ethidium bromide–COF–ClO_4 (2.60×10^{-5} S cm^{-1}).[28] As observed from Table S2 (Supporting Information), Li contents of many MOF-/COF-based QSSEs are in the range of 0.32–5.4 wt%, and the solvent/plasticizer amount generally occupies at least 30 wt%, even 70 wt% of the whole weight of QSSEs. However, LGZ with the addition of 6 µL PC corresponds to the PC content of 19.4 wt%, as determined by thermogravimetric analysis (TGA) (Figure S10, Supporting Information). Obviously, such MOF-based QSSEs with low Li content and lean solvent but superior ionic conductivity have rarely been reported. To investigate the electrochemical stability, linear sweep voltammetry (LSV) measurements were conducted. The stable electrochemical windows are located between 2.3 and 4.0 V for these two QSSEs (Figure 4c; Figure S11, Supporting Information) for that there is no observable current response to electrolyte decomposition on account of the electrochemical stability of imidazolate.[26a]

2.3. Insight into the Mechanism of Enhanced Conductivity in LGZ

To clarify the mechanism for the superior conductivity of LGZ, it is essential to figure out the ion conduction behavior in ZIF-4-based QSSEs. As an important parameter for evaluating ion migration capability, Li^+ transference number (TN) was measured by the modified Bruce–Vincent–Evans (BVE) method.[29] LGZ has a Li^+ TN of 0.885, while a lower TN of 0.512 is obtained for LCZ (Figure 4d,e), suggesting that LGZ has a better ion migration capability and lower polarization. Moreover, EIS curves of the two QSSEs both still show a semicircle with an inclined plot at −56.6 °C (Figure S12, Supporting Information). The corresponding ionic conductivity of LGZ is 5.96×10^{-6} S cm^{-1} and also higher than that of LCZ (i.e., 4.51×10^{-7} S cm^{-1}). These results illustrate that LGZ can still deliver splendid ionic conductivity at low temperature.

To further probe the ionic conduction mechanism, the symmetric cell with a commercial polypropene (PP) separator (Celgard 2400) and 6 µL of 2.9 mol L^{-1} LiTFSI/PC liquid electrolyte (corresponding to 0.12 wt% Li in QSSEs with the addition of 6 µL PC) was also examined. In this case, the ion migration occurs only along the pore surface separator. We found that the Nyquist plot of the PP separator contains a semicircle at high frequency and a straight line at low frequency. Its ionic resistance reaches up to $\approx 2.5 \times 10^4$ Ω (Figure S13, Supporting Information) and its corresponding ionic conductivity is 2.04×10^{-7} S cm^{-1} at 30 °C, which is much lower than that of LGZ. Furthermore, this cell displays a disordered EIS curve (Figure S14, Supporting Information) at −56.6 °C, implying that ion motion cannot proceed through the surface of the PP separator owing to the freezing of the liquid electrolyte (the melting point of PC is −48.8 °C) despite the freezing-point-depression phenomenon with the addition of LiTFSI (Figure S15, Supporting Information).

These results indicate that the ion motion in LGZ is different from the conventional PP separator, where solvated ions move on the surface. This means that the ion conduction in LGZ has another pattern apart from the surface form. The previous studies validated that N species in imidazole groups can interact with Li^+ via weak electrostatic force,[26a,30] regulate Li^+ flux,[31] and promote Li^+ conduction.[26a,31] In addition, glassy materials can

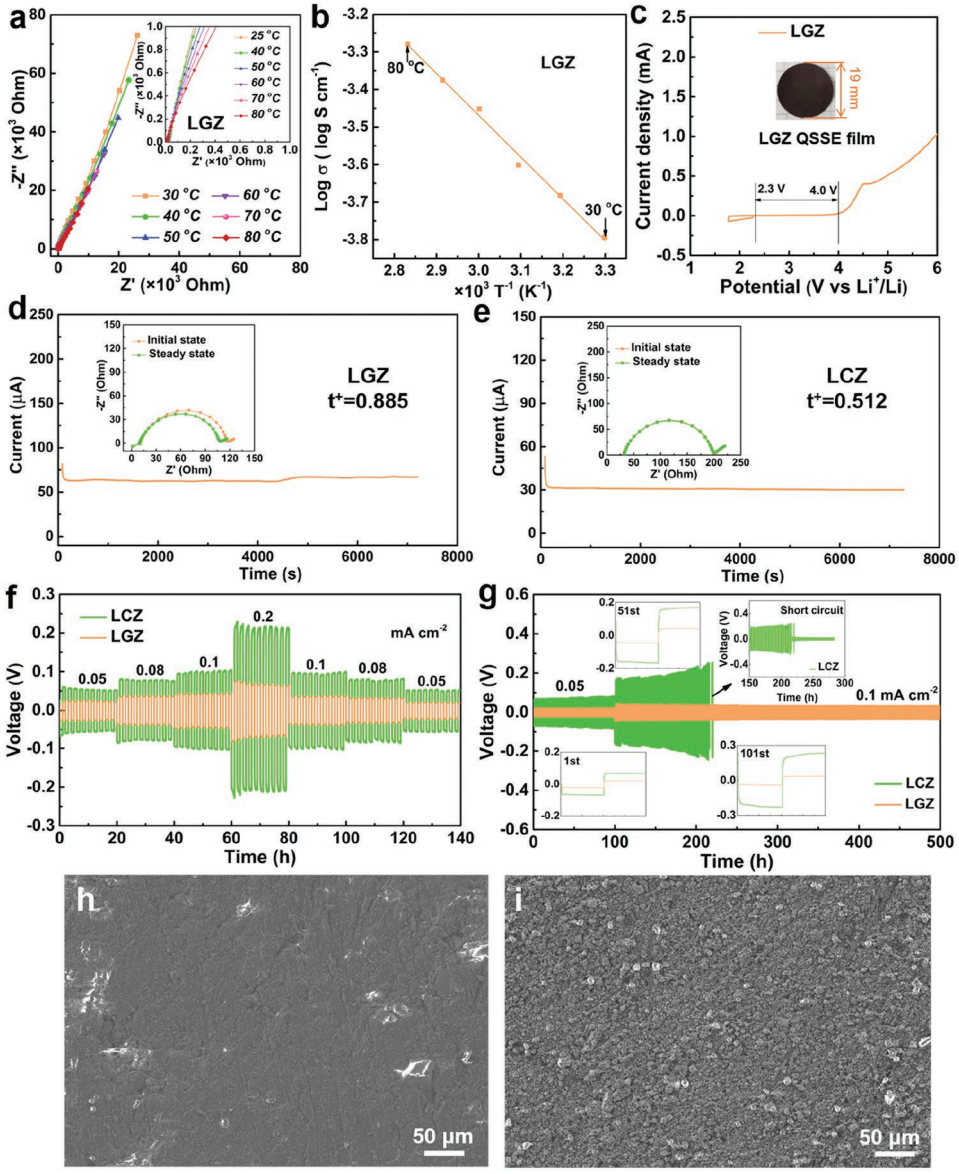

Figure 4. a) Nyquist plots for LGZ from 30 to 80 °C (inset: enlarged Nyquist plots of LGZ film). b) Temperature-dependent conductivity plot of LGZ. c) LSV of the Li|LGZ|ss cell (inset: LGZ film). d,e) Current–time curves of d) Li|LGZ|Li and e) Li|LCZ|Li symmetric cells at 10 mV of polarization (inset: EIS at initial and steady states). f) Rate performance and g) cycling stability of Li plating/stripping for Li|LGZ|Li and Li|LCZ|Li symmetric cells. h,i) SEM images of Li anodes for h) LGZ (after 500 h) and i) LCZ (after 217 h) for plating/stripping tests after cycling stability tests, respectively.

afford the isotropic pathway with reduced impedance for ions' transfer.[15] Thus, there is a wealth of opportunities that Li^+ could conduct throughout the glassy MOF without the limitation of grain boundaries found in crystalline ZIF-4. We speculate that Li^+ could not only conduct on the surface but also inside of ZIF-4 glass along the imidazole frameworks. More in-depth and systematic investigation is ongoing to elucidate the Li-ion conduction mechanism, which will be covered in our upcoming papers.

2.4. Symmetric and Full Cell Characterizations

Li dendrites are generated by inhomogeneous local electric and ionic fields stemming from the differences between diffusion rate and deposition rate of Li^+.[32] Fortunately, grain boundary-free and isotropy properties render LGZ with fast Li^+ flux and uniform distribution, ensuring uniform Li deposition and thus avoiding the formation of Li dendrite.[13,33] Therefore, we verified the advantages of LGZ for Li dendrite suppression in symmetric cells as follows. Figure 4f describes the time-dependent voltage variations of glassy and crystalline QSSEs under stepwise varying current densities. LGZ bears lower polarization voltages of ±23.6, ±35.3, ±41.5, and ±66.3 mV at 0.05, 0.08, 0.1, and 0.2 mA cm^{-2} compared with LCZ. When the current density resumes to 0.05 mA cm^{-2}, a low polarization voltage reappears and even decreases to ±19.5 mV. Long-term cycling tests of Li plating/stripping for both two QSSEs are depicted in Figure 4g. In the initial 100 h, LGZ only exhibits a polarization

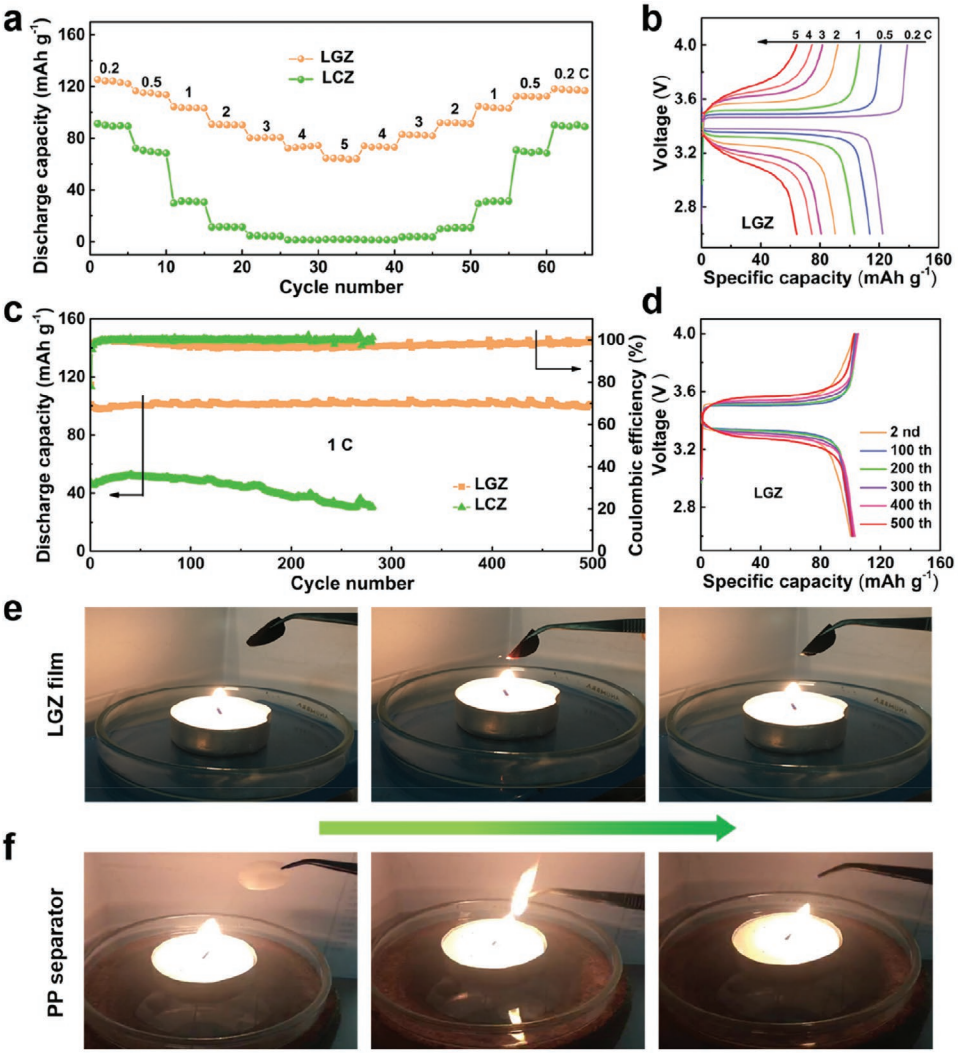

Figure 5. a) Rate performance and c) cycling stability of $LiFePO_4$|LGZ|Li and $LiFePO_4$|LCZ|Li full cells. b,d) Charge/discharge profiles of $LiFePO_4$|LGZ|Li full cells at various current densities and 1 C, respectively. e,f) Combustion behaviors of e) LGZ SSEs film and f) PP separator, respectively.

voltage of ±21.4 mV at 0.05 mA cm^{-2}, obviously lower than that of LCZ (i.e., ±69.0 mV). Upon increasing to 0.1 mA cm^{-2}, the voltage–time curve remains stable with a polarization voltage of ±35.0 mV for another 400 h, whereas LCZ shows a growing voltage fluctuation exceeding ±168.3 mV, and a short circuit indicates cell failure after 217 h. SEM images show that Li metal anode has a smooth surface in Li|LGZ|Li cell, while the counterpart is rather rough in Li|LCZ|Li cell, as exhibited in Figure 4h,i and in Figure S16 (Supporting Information). These results demonstrate that LGZ possesses superior compatibility with Li metal and excellent dendritic suppression in contrast with LCZ.

As a proof-of-the-concept demonstration of our proposed QSSEs, full cells, $LiFePO_4$|LGZ|Li, were assembled to investigate their practicability for LMBs. In full cells, EIS was first tested at various PC volumes and $LiFePO_4$|LGZ|Li with 6 µL has the smallest charge-transfer resistance in agreement with the situation of ss|QSSEs|ss configuration (Figure S17, Supporting Information). Rate performance was conducted for assessing fast-charging property.[34] For these two types of QSSEs, the fast-charging property is mainly influenced by ion conductivity in view of the same chemical composition. As illustrated in **Figure 5**a, LGZ displays specific capacities of 124.3, 115.1, 103.5, 90.4, 80.6, and 73.5 mAh g^{-1} at stepwise current densities of 0.2, 0.5, 1, 2, 3, and 4 C (1 C = 170 mA g^{-1}). Even at 5 C, a capacity of 64.7 mAh g^{-1} can still be achieved, corroborating splendid fast-charging capability. It is worth noting that the capacity basically recovers to the original level when current density switched back to 0.2 C, illustrating the outstanding structural stability of LGZ. Impressively, LGZ still exhibits clear charge/discharge plateaus at 5 C (Figure 5b). In contrast, LCZ delivers lower capacities at corresponding current densities, and especially at 4 and 5 C, the capacities are merely 1.8 and 1.5 mAh g^{-1}, respectively. It could be inferred that high ion conductivity and high TN of LGZ generated an exceptional rate performance. The long-period cycling performance is revealed in Figure 5c. Strikingly, LGZ displays an initial capacity of 101.2 mAh g^{-1} and maintains a steady and high capacity of 101.4 mAh g^{-1} at 1 C after 500 cycles with a capacity retention of near 100%.

In a stark contrast, an initial low capacity of 47.2 mAh g^{-1} is delivered for LCZ, although the capacity undergoes an increase of 52.8 mAh g^{-1} and then gradually decays to 30.7 mAh g^{-1} after 280 cycles. Galvanostatic charge/discharge profiles overlap well (Figure 5d), also indicating that LGZ film owns excellent electrochemical stability. The electrochemical performance of LGZ also outperforms the previously explored MOF-/COF-based QSSEs, e.g., $LiClO_4$@HKUST-1,[22] Li^+/exchanged MOF-688[26b] (Table S2, Supporting Information) and dCOF-ImTFSI-60.[25b] In general, we only loaded the Li content of 0.12 wt% into ZIF-4 glass with the employed PC amount of 6 µL (19.4 wt% occupying the total LGZ) to realize remarkable electrochemical performance, which is tentatively ascribed to the features of ZIF-4 glass including isotropic properties and the inexistence of grain boundary. Undoubtedly, the design of this novel electrolyte also has fast-charging capability, and reduces the fabrication cost and enhances the energy density of quasi-solid-state batteries. Safety concerns remain one of the mostly worrying issues for the implementation of LMBs. As shown in Figure 5e,f, once the ignited LGZ membrane is moved away from the fire, the ignition point quickly extinguishes and no subsequent combustion occurs, while the PP separator fiercely burns with a bright flame, clearly illuminating the prominent flameproof function of LGZ. The outstanding fireproof property of LGZ is beneficial to boost the security of LMBs.

3. Conclusion

In summary, we demonstrated the prominent performance of MOF glass as QSSEs' matrix for LMBs. The transformation of crystalline ZIF-4 into a glass reduces grain boundaries via the melt-quenching process, leading to isotropic pathways for ion migration compared with dense crystalline ZIF-4. The rate performance and long-run cyclability of plating/stripping tests corroborate the outstanding compatibility with Li anodes and suppression of Li dendrites for glassy ZIF-4. Impressively, LGZ, only containing 0.12 wt% Li content and a little PC (19.4 wt%), delivers an exceptional rate performance, superior long-life cycling stability, and high specific capacity, far exceeding LCZ and the majority of reported MOF-/COF-based QSSEs. And LGZ also possesses a low-temperature ionic conductivity and a prominent fireproof property. Our finding demonstrated that MOF glasses to have a bright future as QSSEs for achieving high-performance quasi-solid-state batteries.

4. Experimental Section

Experimental procedures can be found in the Supporting Information.

Supporting Information

Supporting Information is available from the Wiley Online Library or from the author.

Acknowledgements

This work was supported by the National Natural Science Foundation of China (Grant No. 51972270). G.J. acknowledges the sponsorship from China Scholarship Council. F.X. acknowledges support by the Alexander von Humboldt Foundation. S.K. acknowledges support by the DFG (Grant No. KA 1698/27-1) and BMBF excellence center KaSiLi.

Open access funding enabled and organized by Projekt DEAL.

Conflict of Interest

The authors declare no conflict of interest.

Data Availability Statement

Research data are not shared.

Keywords

lithium-metal batteries, metal–organic frameworks, metal–organic framework glass, quasi-solid-state electrolytes, ZIF-4

Received: May 6, 2021
Revised: July 9, 2021
Published online: August 3, 2021

[1] a) H. Furukawa, K. E. Cordova, M. O'Keeffe, O. M. Yaghi, *Science* **2013**, *341*, 1230444; b) H. X. Zhong, K. H. Ly, M. C. Wang, Y. Krupskaya, X. C. Han, J. C. Zhang, J. Zhang, V. Kataev, B. Buchner, I. M. Weidinger, S. Kaskel, P. Liu, M. W. Chen, R. H. Dong, X. L. Feng, *Angew. Chem., Int. Ed.* **2019**, *58*, 10677; c) J. D. Evans, V. Bon, I. Senkovska, H. C. Lee, S. Kaskel, *Nat. Commun.* **2020**, *11*, 2690.

[2] a) S. Krause, V. Bon, I. Senkovska, U. Stoeck, D. Wallacher, D. M. Tobbens, S. Zander, R. S. Pillai, G. Maurin, F. X. Coudert, S. Kaskel, *Nature* **2016**, *532*, 348; b) S. Krause, V. Bon, U. Stoeck, I. Senkovska, D. M. Toebbens, D. Wallacher, S. Kaskel, *Angew. Chem., Int. Ed.* **2017**, *56*, 10676; c) B. Liang, X. Zhang, Y. Xie, R. B. Lin, R. Krishna, H. Cui, Z. Li, Y. Shi, H. Wu, W. Zhou, B. Chen, *J. Am. Chem. Soc.* **2020**, *142*, 17795.

[3] T. Simon-Yarza, A. Mielcarek, P. Couvreur, C. Serre, *Adv. Mater.* **2018**, *30*, 1707365.

[4] a) Q. Wang, D. Astruc, *Chem. Rev.* **2020**, *120*, 1438; b) D. D. Wang, D. L. Jana, Y. L. Zhao, *Acc. Chem. Res.* **2020**, *53*, 1389.

[5] a) E. M. Miner, M. Dinca, *Phil. Trans. R. Soc., A* **2019**, *377*, 20180225; b) C. Li, L. Liu, J. L. Kang, Y. Xiao, Y. Q. Feng, F. F. Cao, H. Zhang, *Energy Storage Mater.* **2020**, *31*, 115; c) R. Zhao, Y. X. Wu, Z. B. Liang, L. Gao, W. Xia, Y. S. Zhao, R. Q. Zou, *Energy Environ. Sci.* **2020**, *13*, 2386; d) S. S. Park, Y. Tulchinsky, M. Dinca, *J. Am. Chem. Soc.* **2017**, *139*, 13260.

[6] J. Q. Zhou, H. Q. Ji, J. Liu, T. Qian, C. L. Yan, *Energy Storage Mater.* **2019**, *22*, 256.

[7] Y. Du, H. Yang, J. M. Whiteley, S. Wan, Y. Jin, S. H. Lee, W. Zhang, *Angew. Chem., Int. Ed.* **2016**, *55*, 1737.

[8] a) T. Ma, E. A. Kapustin, S. X. Yin, L. Liang, Z. Zhou, J. Niu, L. H. Li, Y. Wang, J. Su, J. Li, X. Wang, W. D. Wang, W. Wang, J. Sun, O. M. Yaghi, *Science* **2018**, *361*, 48; b) L. Zou, C. C. Hou, Z. Liu, H. Pang, Q. Xu, *J. Am. Chem. Soc.* **2018**, *140*, 15393.

[9] a) T. D. Bennett, J. C. Tan, Y. Yue, E. Baxter, C. Ducati, N. J. Terrill, H. H. Yeung, Z. Zhou, W. Chen, S. Henke, A. K. Cheetham, G. N. Greaves, *Nat. Commun.* **2015**, *6*, 8079; b) C. Zhou, L. Longley, A. Krajnc, G. J. Smales, A. Qiao, I. Erucar, C. M. Doherty, A. W. Thornton, A. J. Hill, C. W. Ashling, O. T. Qazvini,

S. J. Lee, P. A. Chater, N. J. Terrill, A. J. Smith, Y. Yue, G. Mali, D. A. Keen, S. G. Telfer, T. D. Bennett, *Nat. Commun.* **2018**, *9*, 5042; c) R. Gaillac, P. Pullumbi, K. A. Beyer, K. W. Chapman, D. A. Keen, T. D. Bennett, F. X. Coudert, *Nat. Mater.* **2017**, *16*, 1149; d) C. Gao, Z. Jiang, P. Wang, L. R. Jensen, Y. Zhang, Y. Yue, **2021**, https://doi.org/10.26434/chemrxiv.14745477.

[10] a) Y. Wang, H. Jin, Q. Ma, K. Mo, H. Mao, A. Feldhoff, X. Cao, Y. Li, F. Pan, Z. Jiang, *Angew. Chem., Int. Ed.* **2020**, *59*, 4365; b) L. Frentzel-Beyme, M. Kloss, P. Kolodzeiski, R. Pallach, S. Henke, *J. Am. Chem. Soc.* **2019**, *141*, 12362.

[11] a) H. Tao, T. D. Bennett, Y. Yue, *Adv. Mater.* **2017**, *29*, 1601705; b) T. D. Bennett, S. Horike, *Nat. Rev. Mater.* **2018**, *3*, 431; c) S. Horike, S. S. Nagarkar, T. Ogawa, S. Kitagawa, *Angew. Chem., Int. Ed.* **2020**, *59*, 6652.

[12] a) Y. Nakao, M. Onoda, T. Sakurai, A. Nakahara, I. Kinoshita, S. Ooi, *Inorg. Chim. Acta* **1988**, *151*, 55; b) C. R. Bhattacharjee, P. K. Choudhury, *Transition Met. Chem.* **1998**, *23*, 561; c) T. T. H. Tran, G. L. Chen, T. K. A. Hoang, M. Y. Kuo, Y. O. Su, *J. Phys. Chem. A* **2017**, *121*, 6925.

[13] D. Cao, X. Sun, Q. Li, A. Natan, P. Xiang, H. Zhu, *Matter* **2020**, *3*, 57.

[14] M. M. Ioanniti, W. E. Tenhaeff, *J. Power Sources* **2017**, *371*, 209.

[15] Q. Zhang, D. Cao, Y. Ma, A. Natan, P. Aurora, H. Zhu, *Adv. Mater.* **2019**, *31*, 1901131.

[16] a) T. D. Bennett, Y. Yue, P. Li, A. Qiao, H. Tao, N. G. Greaves, T. Richards, G. I. Lampronti, S. A. Redfern, F. Blanc, O. K. Farha, J. T. Hupp, A. K. Cheetham, D. A. Keen, *J. Am. Chem. Soc.* **2016**, *138*, 3484; b) A. Qiao, T. D. Bennett, H. Tao, A. Krajnc, G. Mali, C. M. Doherty, A. W. Thornton, J. C. Mauro, G. N. Greaves, Y. Yue, *Sci. Adv.* **2018**, *4*, eaao6827; c) A. Qiao, H. Tao, M. P. Carson, S. W. Aldrich, L. M. Thirion, T. D. Bennett, J. C. Mauro, Y. Yue, *Opt. Lett.* **2019**, *44*, 1623.

[17] Y. Q. Tian, Y. M. Zhao, Z. X. Chen, G. N. Zhang, L. H. Weng, D. Y. Zhao, *Chem. - Eur. J.* **2007**, *13*, 4146.

[18] M. T. Wharmby, S. Henke, T. D. Bennett, S. R. Bajpe, I. Schwedler, S. P. Thompson, F. Gozzo, P. Simoncic, C. Mellot-Draznieks, H. Tao, Y. Yue, A. K. Cheetham, *Angew. Chem., Int. Ed.* **2015**, *54*, 6447.

[19] J. Y. Zhang, L. Longley, H. Liu, C. W. Ashling, P. A. Chater, K. A. Beyer, K. W. Chapman, H. Z. Tao, D. A. Keen, T. D. Bennett, Y. Z. Yue, *Chem. Commun.* **2019**, *55*, 2521.

[20] T. D. Bennett, A. L. Goodwin, M. T. Dove, D. A. Keen, M. G. Tucker, E. R. Barney, A. K. Soper, E. G. Bithell, J. C. Tan, A. K. Cheetham, *Phys. Rev. Lett.* **2010**, *104*, 115503.

[21] R. S. K. Madsen, A. Qiao, J. Sen, I. Hung, K. Chen, Z. Gan, S. Sen, Y. Yue, *Science* **2020**, *367*, 1473.

[22] L. Shen, H. B. Wu, F. Liu, J. L. Brosmer, G. Shen, X. Wang, J. I. Zink, Q. Xiao, M. Cai, G. Wang, Y. Lu, B. Dunn, *Adv. Mater.* **2018**, *30*, 1707476.

[23] a) M. Wang, J. Liu, C. Guo, X. Gao, C. Gong, Y. Wang, B. Liu, X. Li, G. G. Gurzadyan, L. Sun, *J. Mater. Chem. A* **2018**, *6*, 4768; b) G. Ren, Z. Li, W. Yang, M. Faheem, J. Xing, X. Zou, Q. Pan, G. Zhu, Y. Du, *Sens. Actuators, B* **2019**, *284*, 421.

[24] a) F. Hillman, J. M. Zimmerman, S.-M. Paek, M. R. A. Hamid, W. T. Lim, H.-K. Jeong, *J. Mater. Chem. A* **2017**, *5*, 6090; b) M. R. Ryder, B. Civalleri, T. D. Bennett, S. Henke, S. Rudic, G. Cinque, F. Fernandez-Alonso, J. C. Tan, *Phys. Rev. Lett.* **2014**, *113*, 215502.

[25] a) G. Zhang, Y. Hong, Y. Nishiyama, S. Y. Bai, S. Kitagawa, S. Horike, *J. Am. Chem. Soc.* **2019**, *141*, 1227; b) Z. Li, Z. W. Liu, Z. Y. Li, T. X. Wang, F. L. Zhao, X. S. Ding, W. Feng, B. H. Han, *Adv. Funct. Mater.* **2020**, *30*, 1909267.

[26] a) Y. Hu, N. Dunlap, S. Wan, S. Lu, S. Huang, I. Sellinger, M. Ortiz, Y. Jin, S. H. Lee, W. Zhang, *J. Am. Chem. Soc.* **2019**, *141*, 7518; b) W. Xu, X. Pei, C. S. Diercks, H. Lyu, Z. Ji, O. M. Yaghi, *J. Am. Chem. Soc.* **2019**, *141*, 17522.

[27] Z. Li, Z. W. Liu, Z. J. Mu, C. Cao, Z. Y. Li, T. X. Wang, Y. Li, X. S. Ding, B. H. Han, W. Feng, *Mater. Chem. Front.* **2020**, *4*, 1164.

[28] Z. B. Guo, Y. Y. Zhang, Y. Dong, J. Li, S. W. Li, P. P. Shao, X. Feng, B. Wang, *J. Am. Chem. Soc.* **2019**, *141*, 1923.

[29] K. M. Abraham, Z. Jiang, B. Carroll, *Chem. Mater.* **1997**, *9*, 1978.

[30] R. D. Corder, S. C. Dudick, J. E. Bara, S. A. Khan, *ACS Appl. Polym. Mater.* **2020**, *2*, 2397.

[31] a) C. Li, S. Liu, C. Shi, G. Liang, Z. Lu, R. Fu, D. Wu, *Nat. Commun.* **2019**, *10*, 1363; b) G. Sun, J. Guo, H. Niu, N. Chen, M. Zhang, G. Tian, S. Qi, D. Wu, *RSC Adv.* **2019**, *9*, 40084.

[32] a) Z. Wang, Z. Sun, J. Li, Y. Shi, C. Sun, B. An, H.-M. Cheng, F. Li, *Chem. Soc. Rev.* **2021**, *50*, 3178; b) X.-B. Cheng, R. Zhang, C.-Z. Zhao, Q. Zhang, *Chem. Rev.* **2017**, *117*, 10403.

[33] Y. Li, D. Cao, W. Arnold, Y. Ren, C. Liu, J. B. Jasinski, T. Druffel, Y. Cao, H. Zhu, H. Wang, *Energy Storage Mater.* **2020**, *31*, 344.

[34] a) G. S. Jiang, X. S. Xu, H. J. Han, C. Z. Qu, H. Repich, F. Xu, H. Q. Wang, *Nano Res.* **2020**, *13*, 2763; b) G. Jiang, Y. Qiu, Q. Lu, W. Zhuang, X. Xu, S. Kaskel, F. Xu, H. Wang, *ACS Appl. Mater. Interfaces* **2019**, *11*, 41188.